International Journal of Heat and Mass Transfer 64 (2013) 792–801

Contents lists available at SciVerse ScienceDirect

International Journal of Heat and Mass Transfer

journal homepage: www.elsevier.com/locate/ijhmt

A parametric study of heat transfer in an air-cooled heat sink enhanced by actuated plates

Youmin Yu, Terrence Simon *, Tianhong Cui

Department of Mechanical Engineering, University of Minnesota, 111 Church Street SE, Minneapolis, MN 55455, USA

ARTICLE INFO

Article history:
Received 24 February 2012
Received in revised form 21 April 2013
Accepted 26 April 2013
Available online 3 June 2013

Keywords:
Heat transfer with agitation
Heat sink
Agitator plate
Electronics cooling

ABSTRACT

Heat transfer in air-cooled heat sinks must be improved to meet thermal management requirements of modern microelectronics devices. This need is addressed by putting agitator plates into channels of a heat sink so that heat transfer is enhanced by agitation. A proof-of-concept exercise was computationally conducted in a single channel consisting of uniform-temperature base and two side walls and an adiabatic fourth wall. The channel side walls are fins of the heat sink fin array. The agitator plate is within the channel. Air flows through the channel and the agitator plate generates periodic motion in a transverse direction to the air flow and to the channel surface. Turbulence is generated along the tip of the agitator plate due to its periodical motion, resulting in substantial heat transfer enhancement in the channel. Heat transfer is enhanced by 61% by agitation for a representative situation. Translational operation of the plate induces 33% more heat transfer than a corresponding flapping operation. Heat transfer on the base surface increases sharply as the tip gap size between it and the agitator plate tip is decreased, while heat transfer on the sidewalls is insensitive to the tip gap size. Heat transfer from the channel wall to the flow increases linearly with increases of amplitude or frequency of the agitator plate. The primary operational parameter to the problem is the product of amplitude and frequency, with amplitude being slightly more influential than frequency.

1. Introduction

Air-cooled heat sinks have been attracting continued investigation due to their high reliability, simplicity, and low cost. Various configurations of air-cooled heat sinks have been investigated. Teertstra et al. [1] developed an analytical model, based on developing flow and fully-developed flow, to predict average heat transfer rates for forced convection in channels of plate-fin heat sinks. Their model calculated average Nusselt numbers as functions of heat sink geometry and air flow velocity. The model was validated for heat sinks of high fin-height-to-fin-spacing ratios. Duan and Muzychka [2] experimentally studied developing laminar flow in rectangular channels of a plate-fin heat sink having various channel dimensions and air flow velocities. Air flow was downwardly impinged to the center of the heat sink and allowed to depart the channels at the two ends of the heat sink. They proposed a simple correlation, $Nu_{D_h} = 0.49L^{*-1/2}$ with $L^* = (L/2)/(D_h \mathrm{Re}_{D_h} \mathrm{Pr})$, for predicting mean heat transfer coefficients. By placing an adiabatic shroud above the fin tips of a plate-fin heat sink, Sparrow and Kadle [3] experimentally investigated effects of gap size between the fin tips and the shroud on turbulent heat transfer in the heat sink. They reported that heat transfer coefficients decreased to 85, 74, and 64 percent of that of a zero gap size case as the gap size was increased to 10%, 20%, and 30% of the fin height, respectively. El-Sayed et al. [4] extended a similar study to surface-roughened shrouds and even larger gap sizes. They found that surface-roughened shrouds induced higher Nusselt numbers than did plain shrouds and the effects of the shrouds on heat transfer diminished when the gap size was greater than the fin height. With a fixed total space for the combination of fan and heat sink and a fixed fan power for cooling the CPUs of desktop computers, Saini and Webb [5] discussed the effects of air flow configuration. Air flow introduced centrally to downwardly impinge on the heat sink removed 19% more heat than air flow passing laterally. Moffat [6] compared common approaches for describing thermal resistances of heat sinks and advocated heat exchanger theory as the most appropriate methodology for heat sink analysis. Ortega et al. [7] showed that an effectiveness-NTU approach more accurately characterized heat transfer performance of heat sinks than commonly-used overall thermal resistance approaches. Bar-Cohen and Iyengar [8] emphasized sustainability, in that not only thermal design and pumping power but also material costs and operating life must be considered in design so that least-energy-consumed heat sinks are achieved. Heat transfer capacity of air-cooled heat sinks is known to be much less than capacities of liquid or boiling cooling

* Corresponding author. Tel.: +1 612 625 5831; fax: +1 612 624 5230.
E-mail address: tsimon@me.umn.edu (T. Simon).

0017-9310/$ - see front matter © 2013 Elsevier Ltd. All rights reserved.
http://dx.doi.org/10.1016/j.ijheatmasstransfer.2013.04.065

Nomenclature

A	peak operational amplitude, mm
a_0	operational amplitude, mm
D	agitator plate thickness, mm
D_h	channel hydraulic diameter, mm
f	operational frequency, Hz
G	tip gap size, mm
H	fin height, *mm*
h	convective heat transfer coefficient, W/m^2 K
Nu	Nusselt number, hD_h/k
p	amplitude–frequency product, m/s
q''	heat flux, W/m^2
Re	Reynolds number, Re = VD_h/v
s	heat transfer area of fin surface
T	temperature of fin surface or air flow, K
t	time, sec
V	channel flow or agitation velocity, m/s
W	fin channel width, mm

Subscripts

air	air flow
base	fin base
fin	fin
wall	fin wall

devices. But there is a reluctance to move to the more complex liquid or boiling systems. Therefore heat transfer of air-cooled heat sinks must be continually improved to meet the thermal management requirements of modern microelectronics devices, as noted by Rodgers et al. [9].

Piezoelectrically-driven agitators or fans have recently been considered for heat transfer enhancement. This is attributed to the large deflections that piezoelectric materials may generate and their small power consumption at resonant frequencies. A common piezo-fan is a thin plate with piezoelectric material bonded to it, as studied by Toda and Osaka [10]. When excited by an alternating voltage, the piezo-material contracts and expands, causing the plate to deflect accordingly. Another type of piezo-fan is a piezo-bow configuration proposed by Joshi and Priya [11]. A piezo-stack contracts and expands along its axial direction and the bow structure transforms this motion into deflections perpendicular to the stack's axial direction. Deflections generated by either type of agitator can stir the air surrounding it, resulting in enhanced mass or heat transfer.

Kim et al. [12] measured the air flow generated by an agitator plate using phase-resolved particle image velocimetry and smoke visualization techniques. They observed that within each oscillation cycle, a pair of counter-rotating vortices was generated and a high-velocity region was formed between the counter-rotating vortices. They concluded that the flow features near the plate tip were quite complicated. Eastman and Kimber [13] measured the flow field as induced by a single piezo-fan using 2-D particle image velocimetry. They found that larger amplitudes generated more repeatable and predictable vortex patterns.

Shmidt [14] measured local and average mass transfer on a surface located perpendicular to a dual piezo-plate arrangement using the naphthalene sublimation technique. The two plates were operated 180° out of phase and three plate-to-surface separation distances were discussed. The maximum local Sherwood numbers occurred at two locations, the projection locations of the tips of the plates when they were in their mean position. The average Sherwood number was relatively insensitive to the plate-to-surface distance.

Kimber et al. [15] and Kimber and Garimella [16] measured local heat transfer coefficients on a surface that was perpendicular to a piezo-fan. The fan-tip-to-surface distance, fan frequency, and amplitude were shown to affect the heat transfer coefficients significantly. Kimber and Garimella [17] extended this to similar investigations with arrays of piezo-fans. Liu et al. [18] measured heat transfer on a flat surface under different fan-to-surface arrangements. They concluded that heat transfer augmentation was due to air flow entrained during each oscillation cycle and by jet-like air streams at the fan tip; with the two modes of heat transfer enhancement, entrainment and jetting nearly equal.

Açıkalın et al. [19] developed a simplified, 2-D CFD model to study the flow field and heat transfer as induced by a piezo-fan. They documented changes in local circulation and vortices as the fan-tip-to-heat-transfer-surface distance was varied. The relationships between flow features and heat transfer enhancement were discussed. Abdullah et al. [20] conducted 2-D CFD computations of heat transfer enhancement on a surface by flow induced by a piezo-fan. The fan was parallel to the surface when at its zero-deflection position. The fluid vorticity and temperature contours were generated near the fan tip, then moved downstream along the fan axis and away from the fan. Lin [21] analyzed heat transfer and fluid flow induced by a piezo-fan near a flat heated surface. His 3-D CFD simulations showed that interaction between the normal force exerted on the air surrounding the moving blade and the impingement jet flow produced at the blade tip prompts formation of two counter-rotating screw-type flow circulations, one at each edge of the blade.

Because of the 3-D feature of the induced fluid flow, piezo-fans are integrated with heat sinks to enhance heat transfer. Petroski et al. [22] optimized the configuration of an air-cooled heat sink coupled with piezo-fans so that the latter improved heat transfer on not only the base surface but also the fin surfaces. Ma et al. [23] investigated a cooling system composed of a single-channel heat sink and a piezo-fan within the heat sink channel. Large velocity and temperature gradients next to the mid section of the fin base and side wall were predicted by 3-D simulations and confirmed by experiments. Effects of operating frequency, fan amplitude, fan arrangement, and power consumption were analyzed to optimize the design of the cooling system. Abdulla et al. [24,25] integrated multiple piezo-fans with a fined heat sink for microelectronics cooling. With the given operating frequency, they reported that the tip gap, operating amplitude, and orientation of the piezo-fans affect heat transfer significantly. Smaller tip gap, larger amplitude, and an orientation perpendicular to both heat-sink base and fins induce higher heat transfer enhancement. Ma et al. [26] also developed multiple piezo-fans operating at 20–50 Hz frequency to cool heat sinks with air.

In order to augment heat transfer of high-heat-flux electronic systems, Yeom et al. [27] and Yu et al. [28] integrated piezo-agitators and a blower into a heat sink so that more thermal energy may be dissipated from the heat sink. The blower generates bulk channel flow between fins of the heat sink; the piezo-agitators, vibrating in a transverse direction between the fins, agitate the channel flow. Such integration of channel flow and agitation improves heat transfer on not only the fin bases (channel bases) but also the fin walls (channel side walls). Significant heat transfer enhancement from the integrated system, compared to pure channel flow, was reported. To effectively agitate the channel flow, the vibration of the agitator velocity must be high, comparable to the channel flow

velocity. Yeom et al. [29] developed a series of piezo-driven agitators. The highest vibrating frequency is 1444 Hz and the largest amplitude is 2.1 mm. Yeom et al. [30] experimentally showed that about 55% heat transfer enhancement relative to pure channel flow when vibration of the agitator was with 961 Hz frequency and 1.4 mm amplitude.

The present study is closely related to the investigations reported by Yeom et al. [27] and Yu et al. [28]. This study focuses on effects of various operational parameters of agitator plates on heat transfer enhancement and was conducted by using transient 3-D CFD simulations. In the next sections, the problem is introduced, a description of the numerical scheme is presented, and the results are reported and discussed.

2. Description of problem

The integration of channel flow and agitation was investigated using a representative single-channel heat sink unit and a single agitator plate. The heat sink channel dimensions were first chosen to meet the dissipated heat level with the fan power and overall space limitations, and then were adjusted based on the physical and operational limits of the agitator plate, as learned during the physical tests. Fig. 1 shows the end-view schematic of the channel. It is 3.4 mm wide, 10.2 mm high, and 20 mm long in the streamwise direction. The agitator plate is 0.8 mm thick, 9.2 mm high, and 20 mm long. The nominal tip gap size between the plate and the fin base is 1.0 mm. A fourth wall forms the closed channel. In Fig. 1, the agitator plate is vibrated to the left and right while the channel flow is perpendicular to the page. The agitator plate may be driven to flap by a piezo-patch attached to it or to translate by a piezo-stack and bow structure such as described in the literature [27,29,30]. Both had the same displacement. Air flow enters the heat sink channel at a constant 14.7 m/s velocity. The corresponding Reynolds number, Re, is 2220, based on the hydraulic diameter of the channel. With the described configuration and operational mode, the tip gap size as well as the amplitude and frequency of the agitator plate are varied to find their influence on heat transfer. The results guide toward optimal heat transfer enhancement.

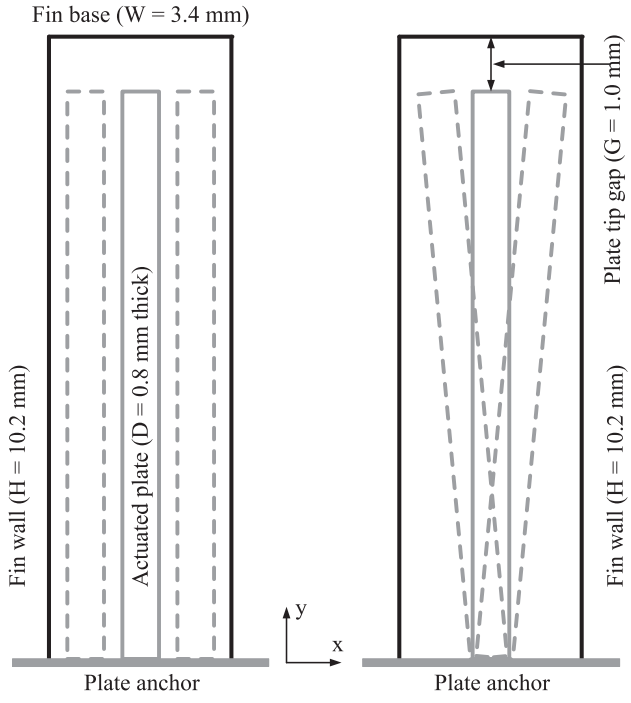

Fig. 1. End-view schematic of the integration of heat sink channel and agitator plate; Left – Translational mode, right – Flapping mode.

3. Numerical simulation

The fluid flow and heat transfer within the channel were modeled using the ANSYS FLUENT software [31]. The geometric model is shown in Fig. 2. The flow passage is the dark region; the agitator plate is the lighter region inside, extending over the entire channel.

Boundary conditions in computations were specified as uniform and constant velocity (14.7 m/s) and temperature (300 K) flow at the channel inlet, uniform and constant pressure (101.3 kPa) at the channel outlet, uniform and constant temperature on the fin base and side walls (350 K), and the three walls of the agitator plate as well as the fourth wall (at the bottom and between the agitator plate and the fin side walls) adiabatic. Air flow is treated as incompressible Newtonian flow with constant properties consistent with 300 K and atmospheric pressure.

User-defined functions and dynamic meshes are employed in order to accurately simulate movement of the agitator plate. Motion of the agitator plate is specified by a user-defined function

$$x = a_0 \sin(2\pi f t) \tag{1}$$

where x is the plate position at time t and a_0 and f are the operational amplitude and frequency, respectively. When operating in the translational mode, the amplitude is

$$a_0 = A \tag{2a}$$

when operating in the flapping mode, the amplitude is

$$a_0 = \frac{y}{H - G} A \tag{2b}$$

in which A is the specified amplitude, y is the height of a point on the plate, H is the fin wall height, and G is the tip gap size. By assigning specific values to A and f in Eqs. (1) and (2), movement of the agitator plate is defined. It is noted that actual piezo-driven flapping is usually first-mode resonant vibration as described in the literature [19,21]. The plate movement is simplified as Eq. (2b). The simplification reduces the computation effort but still essentially keeps the important features of actuator movement.

The flow field must be meshed using dynamic meshes to respond to the movement of the agitator plate. When the plate

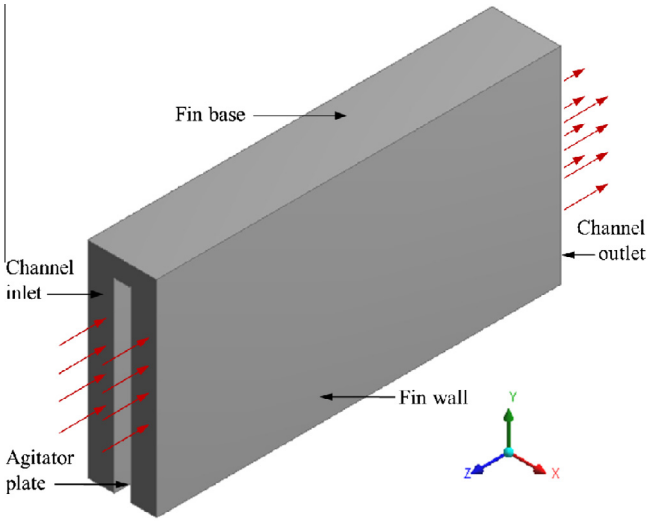

Fig. 2. Geometric model of the CFD simulations – the agitator plate extends through the entire channel.

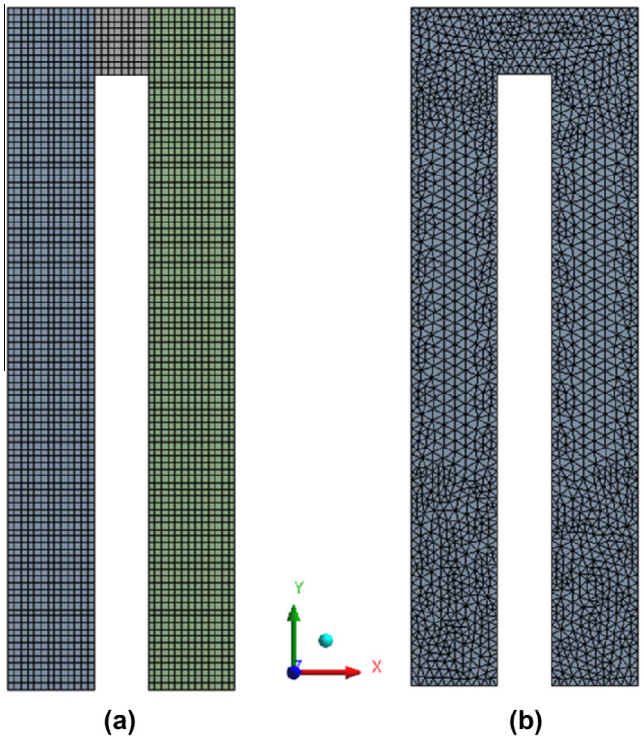

Fig. 3. Dynamic meshing schemes used in the simulations; (a) translational mode, (b) flapping mode.

moves in a translational mode, the flow field is meshed as dynamic hexahedrons and the meshes are adjusted using a layering method, as shown in Fig. 3(a). As the plate moves to right, for instance, mesh layers on the left increase; correspondingly, layers on the right decrease, and meshes directly above the plate tip translate with the plate. When the plate moves in a flapping manner, the flow field is meshed as dynamic tetrahedrons and the meshes are adjusted using remeshing and smoothing methods, as shown in Fig. 3(b). At each time step, all tetrahedral meshes are adjusted according to the position of the plate. Detailed descriptions of the user-defined function, dynamic mesh, layering, remeshing, and smoothing method can be found in the user's manual in the literature [31].

The fluid flow and heat transfer within the channel were computed using a transient pressure-based solver and a realizable k–ε turbulence model with enhanced wall treatment near the walls. Among the solution methods is the SIMPLEC algorithm to solve pressure–velocity coupling, a standard interpolation algorithm to calculate pressure, a second-order upwind method to discretize the convection terms, a Green-Gauss node-based method to discretize the gradient terms, and a first-order implicit method to discretize time in the governing equations. Within the solution controls, under-relaxation factors were kept at their default values. The convergence criterion was 10^{-4} for continuity and momentum equations and 10^{-7} for the energy and turbulence equations. The time step was chosen to be 200 steps per operational cycle, i.e., 1.0×10^{-5} s/time step when the plate moved at 500 Hz, 2.5×10^{-6} s/time step when operated at 2000 Hz, to capture the dynamics. Values of the desired parameters were recorded at each time step.

The numerical scheme that ensured mesh-independent results was chosen. Different mesh sizes were used with the chosen time step for a case of $G = 1.0$ mm, $A = 0.7$ mm, and $f = 1000$ Hz. Calculated heat transfer coefficients, h, are summarized in Table 1. Based on convergence of the heat transfer coefficients, mesh counts of 540,936 and 718,383 were employed in the translational and flapping modes, respectively. The corresponding maximum mesh size was 0.10 mm for translation and 0.13 mm for flapping. With the two mesh counts, the wall $y+$ for the wall-adjacent meshes is less than 3.0 in the translation mode and is less than 2.0 in the flapping mode. Since the wall $y+$ is less than 5, the two mesh counts are able to capture the viscous sublayer next to the fin walls.

Converged results must be further validated. A numerical scheme similar to the present scheme was validated against experiments in the literature [28]. In the comparison case [28], the heat sink channel had a comparable geometry to that of the current channel, a similar channel flow velocity (8.0–14.7 m/s), and comparable agitator operation ($A = 0.7$ mm and $f = 500$ Hz). Calculated heat transfer coefficients matched experimental values to within 5.3%. The numerical scheme accurately reproduced the experimental results and, hence, was validated.

With the validation complete, each computation was first run until all variables were periodically stable. Then, one more operational cycle was run to collect the desired parameters.

Heat transfer enhancement on the channel base and side walls is represented by increases of heat transfer coefficients. The average heat flux, q'', on each channel surface and the bulk mean temperature, T_{air}, of the air in the channel were extracted from the computation. Heat transfer coefficients, h, on the channel base and side walls were then calculated by

$$h = q''/(T_{wall} - T_{air}) \tag{3}$$

where $T_{wall} = 350$ K on the channel base and side walls, as specified among the boundary conditions. All results presented are time-mean values over the last stable cycle, unless otherwise specified. It is noted that the calculated h on the left and right fin walls (Fig. 3) are 180° out of phase with one another, but of the same mean value.

4. Results and discussion

The main objective of this program is to augment heat transfer using an agitator plate. The operational mode of the agitator plate is first investigated to determine the mode of agitator movement that enhances heat transfer more. With the operational mode decided, effects of tip gap size and oscillation amplitude and frequency are investigated about a representative condition of $G = 1.0$ mm, $A = 0.7$ mm, and $f = 1000$ Hz. The term "channel flow" in the discussion refers to a case of the same air flow and heat sink channel and agitator plate geometries, but with the agitator plate stationary.

4.1. Effects of operational mode on heat transfer enhancement

Effects of the operational mode were investigated with $G = 1.0$ mm, $A = 0.7$ mm, and $f = 1000$ Hz. Fig. 4 shows heat transfer coefficients on the base and side walls when only channel flow is available for cooling and also when the cooling is augmented by agitation of the plate. Both flapping and translational modes significantly improve heat transfer. The heat transfer coefficient on the fin base is 188 W/m^2 K for channel flow, enhanced by 80% by flapping operation and 138% by translational operation. The heat transfer coefficient on the side wall is 203 W/m^2 K for channel flow, enhanced by 30% by flapping and 61% by translation. The heat transfer coefficient with translation is 33% more than that with flapping on the base and 23% more on the side wall.

The heat transfer enhancement is accompanied by an increase of pumping and agitator power consumption. Yu et al. [32] showed that the pump power accounted for more than 80% of the total power consumption. The pump power may be calculated from

Table 1
Calculated heat transfer coefficients, h (W/m^2 K), with different mesh counts.

Translational mode	Mesh count	7,200	166,188	540,936	1,052,274	1,619,655
	h on fin_wall	305.0	315.7	326.8	330.8	329.4
	h on fin_base	400.2	423.3	460.8	464.2	469.3
Flapping mode	Mesh count	251,549	374,210	536,096	718,383	1,079,552
	h on fin_wall	242.9	255.5	265.7	267.2	265.0
	h on fin_base	303.6	325.1	340.0	342.5	345.8

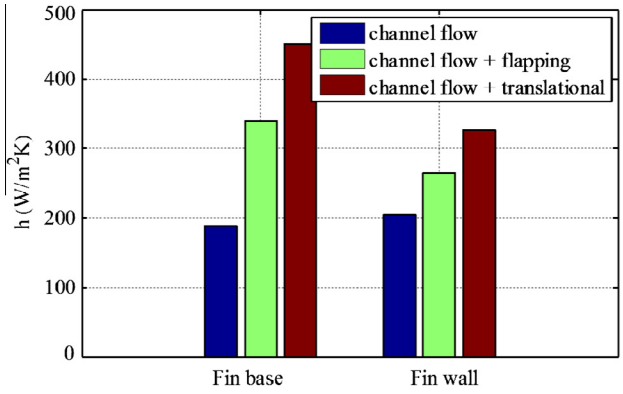

Fig. 4. Comparison of heat transfer coefficients between the two operational modes with G = 1.0 mm, A = 0.7 mm, and f = 1000 Hz.

the total pressure drop across the channel. The pressure drops corresponding to the results in Fig. 4 and their increases relative to the channel flow only case are listed in the first two columns of Table 2. The respective heat transfer enhancement is listed in the seventh and ninth columns. When the same increase of pressure drop is applied to a common turbulent channel flow, the relative heat transfer enhancement may be estimated by:

$$\Delta p \sim V^2 \sim \mathrm{Re}^2 \sim (h^{5/4})^2 \tag{4}$$

21% and 39%, respectively (see fifth column of Table 2). Both heat transfer enhancement values are less than those achieved by flapping and translational agitation. In other words, if power consumption could rise, investing it in agitation generates more turbulence and mixing effects and more heat transfer enhancement than investing it in additional fan flow.

Heat transfer enhancement with either of the two modes may be attributed to transverse turbulence and streamwise unsteadiness generated by periodic motion of the agitator plate. Fig. 5 plots contours of Turbulence Kinetic Energy (TKE) on an *XY* plane and on a *YZ* plane five times during one cycle of translational operation. Fig. 6 is a similar plot, but for the flapping operation. The two figures show the turbulence and unsteadiness generated.

When the agitator plate moves in the transverse direction, air moves accordingly in the transverse direction, in addition to its primary motion in the streamwise direction. Air passes over the top edge of the plate due to the agitation motion and turbulence is generated in the flow at the top edge location. The transverse turbulence is directly related to the velocity of the plate. This is clearly seen in views (a), (c), and (e) of Figs. 5 and 6. At these three times, the agitation velocity, which is the derivative of Eq. (1), reaches its maximum and the TKE values accordingly reach their maxima. The transverse turbulence created subsequently increases heat transfer from the channel surfaces to the air flow, especially from the base and the portions of the side walls next to the base.

Increased heat transfer comes also from streamwise unsteadiness. When the agitator plate moves to the right, channel flow in front of it is accelerated and flow behind it is decelerated, as shown in view (b) of Figs. 5 and 6. The strong flow acceleration does not generate obvious turbulence, but the strong flow deceleration does induce turbulence between the plate surface and the channel walls. Such turbulence is clearly seen in the *YZ* plane in view (b). Similar turbulence is generated in view (d) of Figs. 5 and 6, although the turbulence at this time is on the right side of the agitator plate. The intensity of streamwise turbulence is weaker than that of the transverse turbulence, but it does enhance heat transfer from the channel walls.

For a given amplitude of oscillation, each part of a translating agitator plate moves at that amplitude, whereas only the top edge of a flapper plate moves at that amplitude (see Fig. 1). Accordingly, turbulence generated by the translator is stronger and spreads to a broader region than that generated by the flapper. This explains why heat transfer enhancement by translational operation is higher than that by flapping.

The difference in heat transfer enhancement between the two modes may be seen also in the volumetric-averaged TKE values plotted in Fig. 7. In the channel flow case, a 5.0 m^2/s^2 TKE specified at the channel inlet decays to 4.3 m^2/s^2. This is because the corresponding Reynolds number is 2220 and sustained turbulence production is not expected. The agitator plate boosts the average TKE from 5.0 to 11.2 m^2/s^2 using the flapping operation and to 34.6 m^2/s^2 using the translational operation. Thus, the agitation of the plate clearly induces turbulent-like fluid motion. Again, it is seen that translational operation generates higher and stronger turbulence than does the flapping operation.

Since the translational mode augments heat transfer more than does the flapping mode, the following investigations focus on the translational mode. They document the effects of tip gap size and operational amplitude and frequency.

4.2. Effects of tip gap size on heat transfer enhancement

Effects of the tip gap size between the fin base and the top edge of the agitator plate was studied in the translational mode, with 0.7 mm amplitude, 1000 Hz frequency, and tip gap sizes from 0.5 to 5.0 mm. The results are plotted in Fig. 8, in which the tip gap sizes are normalized by the total plate-to-fin-wall spacing, given as W–D = 3.4–0.8 = 2.6 mm. It is seen that heat transfer is more sensitive to the tip gap size for the fin base than for the side walls and the sensitivity is greater for smaller tip gap sizes.

The turbulence generated along the top edge of the agitator plate is directly related to the agitation velocity

$$V_{\text{agitation}} = \frac{\partial}{\partial t}(a\sin(2\pi f t)) \tag{5}$$

For a given operation, the average agitation speed is expected to be independent of tip gap size. The turbulence levels and effects on heat transfer, however, vary with tip gap size, as shown in Fig. 9. It is noted that in Fig. 9 the plates are at their neutral position and about to move toward the right.

When the tip gap size is small, the generated turbulence quickly transports to the base region, resulting in more heat transfer from the base surface to the air. As the tip gap size increases, the

Table 2
Comparison of heat transfer enhancement between common turbulent channel flow and the agitated channel flow. All changes listed are relative to channel-flow case. Comparison conditions are listed in Fig. 4.

Condition	ΔP_{total} (Pa)	ΔP_{total} change	With common turbulent channel flow			With present agitated channel flow			
			Velocity change	Re number change	htc change	htc on base (W/m^2 K)	htc on base change	htc on wall (W/m^2 K)	htc on wall change
Channel flow	112.8	1.00	1.00	1.00	1.00	188.4	1.00	203.3	1.00
Channel flow + flapping	180.8	1.60	1.27	1.13	1.21	339.6	1.80	264.8	1.30
Channel flow + translational	258.3	2.29	1.51	1.23	1.39	449.2	2.38	327.0	1.61

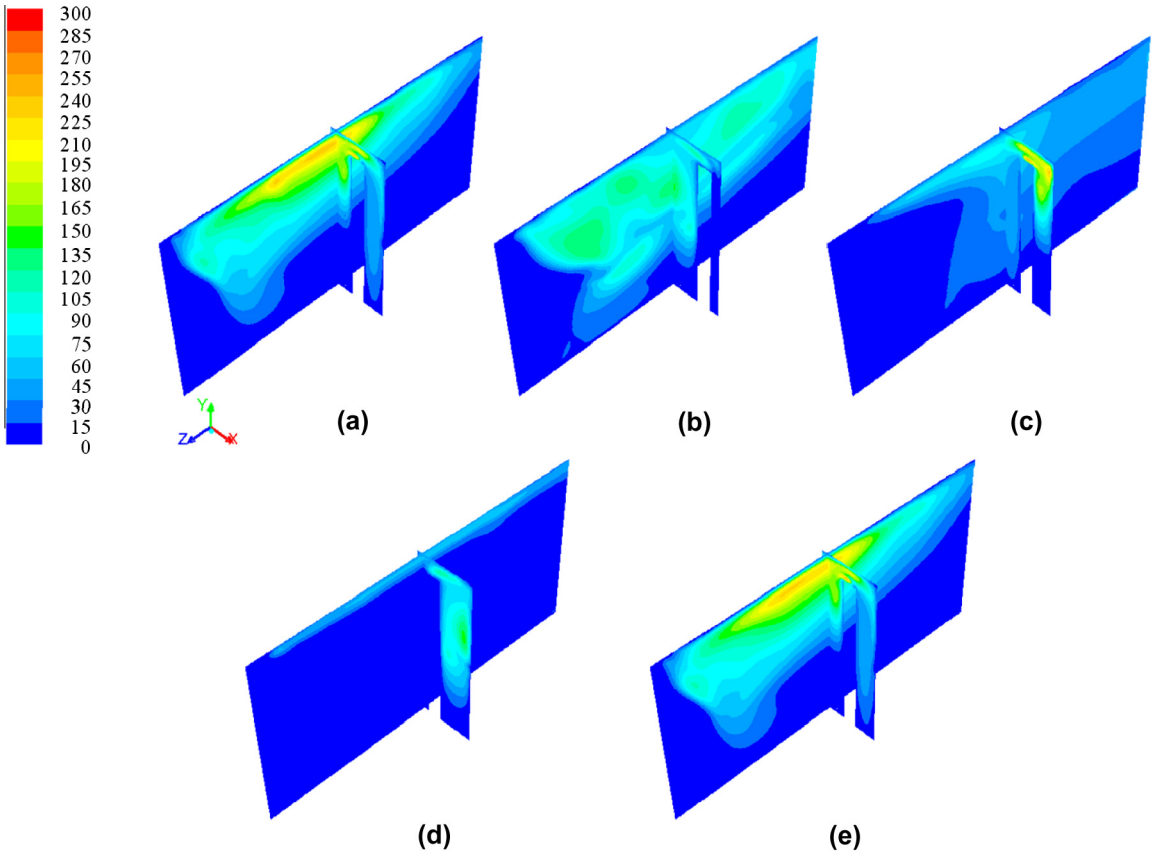

Fig. 5. Contours of TKE [m^2/s^2] on a *YZ* plane (0.3 mm away from the left side wall) and on an *XY* plane (midway along the channel) at various times within one translational cycle; (a) 0%, (b) 25%, (c) 50%, (d) 75%, and (e) 100% (essentially the same as 0%).

turbulence generated and impinging on the base region is reduced. Heat transfer on the base surface, consequently, is decreased. It is noted that the boundary layer thickness in the channel flow is around 0.35 mm, less than the 0.5 mm smallest tip gap size. It is indeed the turbulence generated and advected through the gap region that disrupts the boundary layer to enhance heat transfer on the base surface.

Heat transfer on the side walls is less affected by tip gap size. The total plate-to-fin-wall spacing (*W*–*D*) is not changed for these gap size study cases. However, increasing the tip gap size allows more space for gap flow, lower turbulence production, and a longer time and advection distance for the generated turbulence to decay. As a result, heat transfer on the sidewalls decreases only mildly with increases of the tip gap size.

It is interesting to note that with the 1.0 normalized tip gap size, where the tip gap size is equal to the normal plate-to-fin-wall spacing, plots of heat transfer coefficients with gap size on the base and side walls cross (see Fig. 8). For larger tip gaps, the heat transfer coefficients continue to decrease but the rates are smaller, compared with those for the small tip gap cases.

4.3. Effects of operational amplitude on heat transfer enhancement

Effects of the operational amplitude were studied in the translational mode, with 1.0 mm tip gap size, 1000 Hz frequency, and amplitudes of 0.6–1.0 mm. The results are summarized in Fig. 10. The amplitude is normalized by the 2.6 mm plate-to-fin-wall spacing. Heat transfer coefficients on the base and side walls linearly increase as the amplitude increases. This trend is indicated by Eq. (5) as increasing amplitudes induce greater agitation velocities. Also, heat transfer is higher on the base than on the side walls, which is due to the 1.0 mm tip gap size (0.38 in non-dimensional form). As shown in Fig. 8, when the non-dimensional gap size is less than 1.0, turbulence generated at the agitator plate tip enhances heat transfer more on the base surface than on the side walls.

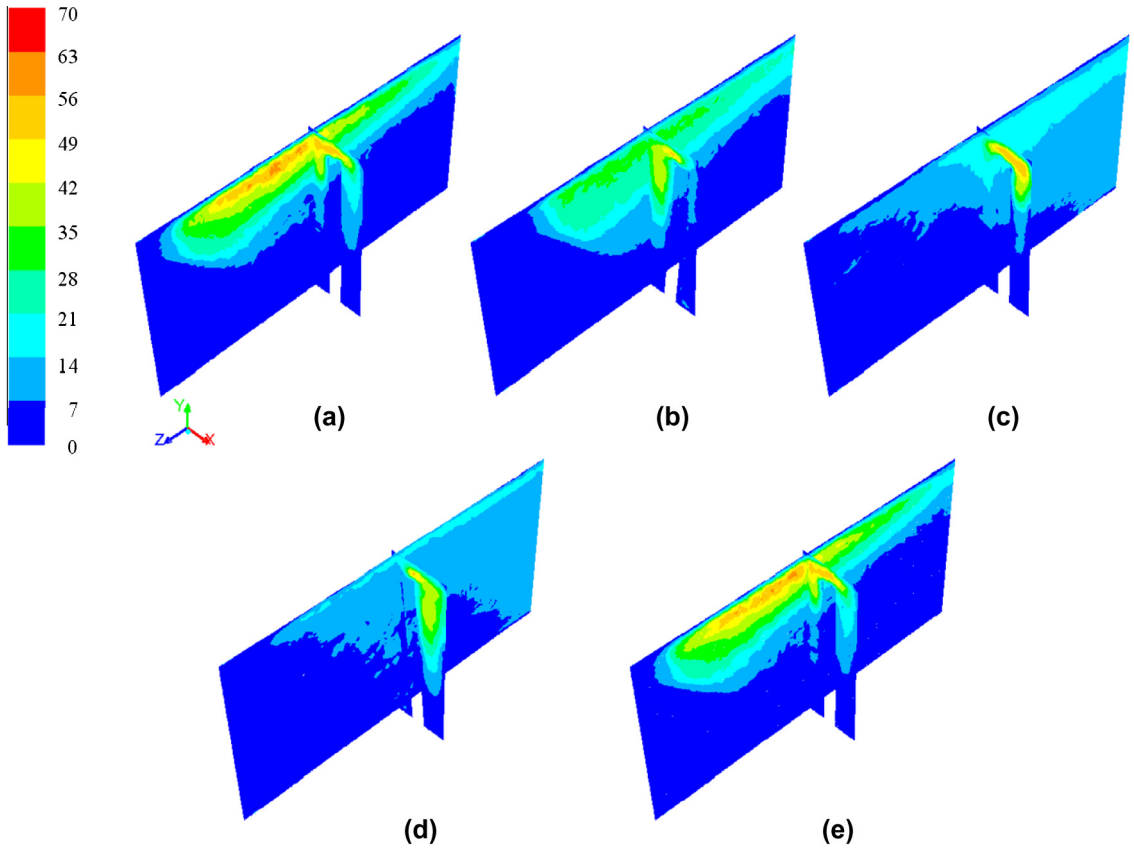

Fig. 6. Contours of TKE [m^2/s^2] on a *YZ* plane (0.3 mm away from the left side wall) and on an *XY* plane (midway along the channel) at various times within one flapping cycle; (a) 0%, (b) 25%, (c) 50%, (d) 75%, and (e) 100% (essentially the same as 0%).

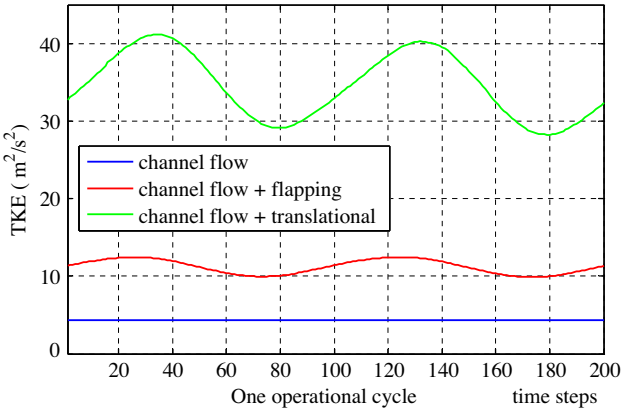

Fig. 7. Volumetric-averaged TKE over one cycle for the two operational modes.

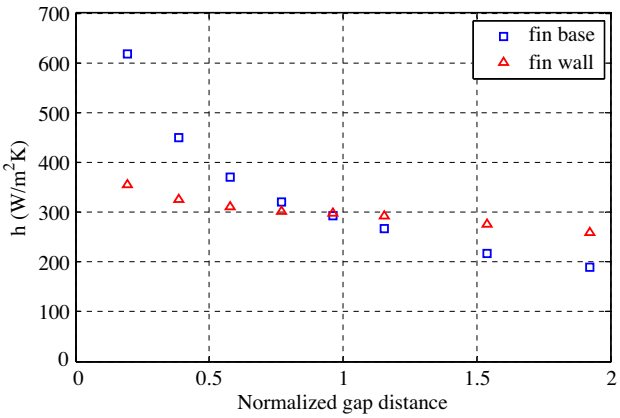

Fig. 8. Heat transfer coefficients with different normalized tip gap sizes.

4.4. Effects of operational frequency on heat transfer enhancement

Effects of the operational frequency were investigated for the translational mode, with 1.0 mm tip gap size, 0.7 mm amplitude, and frequencies of 500–2000 Hz. Fig. 11 shows the results. Heat transfer coefficients on the base and side walls both linearly increase as the frequency increases. This is, again, indicated by Eq. (5) as higher frequencies yield greater agitation velocities. Heat transfer coefficients on the base wall increase with frequency more strongly than those on the side walls. This trend is attributed to the turbulence generated by air flow through the small gap. Higher frequencies generate larger turbulence levels which more easily influence the base wall than the side walls due to nearness to the small tip gap. Higher heat transfer coefficients on the base wall than on the side walls are again attributed to the small, 1.0 mm, tip gap size, as discussed in the previous subsection.

4.5. Effects of operational amplitude–frequency product on heat transfer enhancement

The purpose of this part is to find the relative importance of amplitude and frequency when their product is kept constant. The study was conducted in the translational mode, with 1.0 mm tip gap size, and constant peak agitation velocity, $2\pi Af$, of 4.4 m/s. Four different amplitudes and frequencies with common

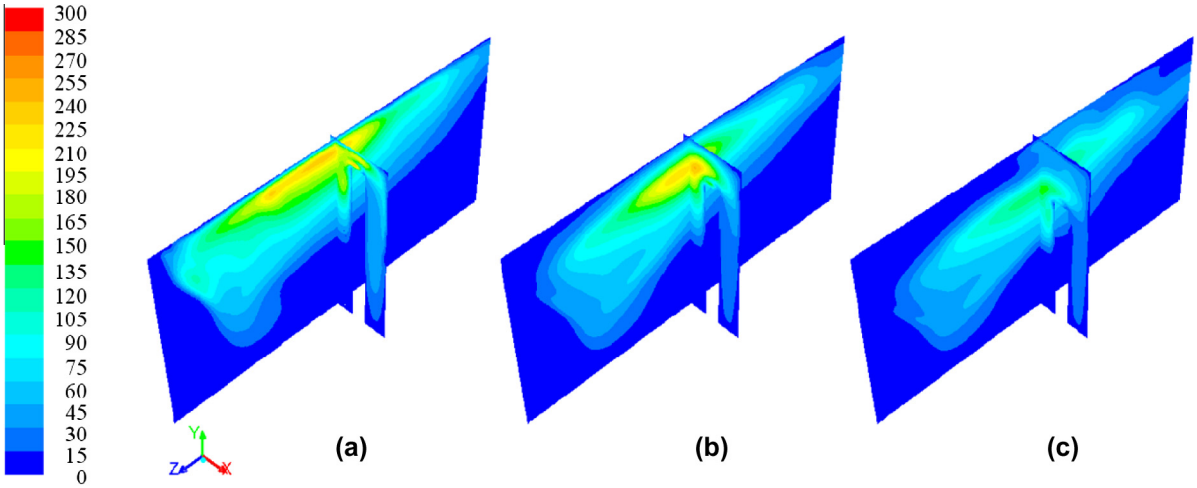

Fig. 9. Contours of TKE [m^2/s^2] on the same *XY* and *YZ* planes, at the same time within the translational cycle, but with different tip gap sizes of (a) 1.0 mm, (b) 2.0 mm, and (c) 3.0 mm, or (a) 0.38, (b) 0.77, and (c) 1.15 in non-dimensional form.

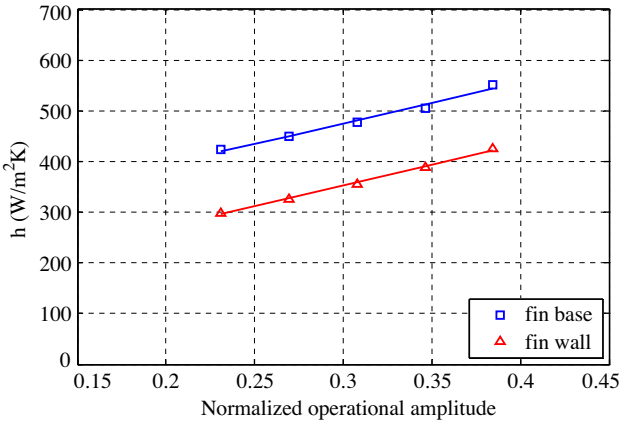

Fig. 10. Heat transfer coefficients with different non-dimensional operational amplitudes; solid lines are linear fits to data.

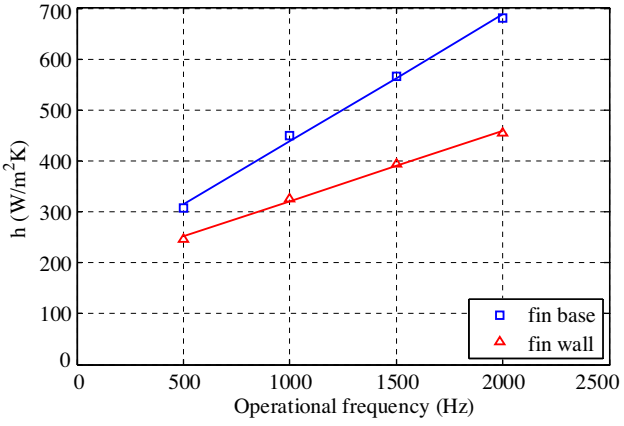

Fig. 11. Heat transfer coefficients with different frequencies; solid lines are linear fits to data.

products were arranged as 1.0 mm and 700 Hz, 0.7 mm and 1000 Hz, 0.5 mm and 1400 Hz, and 0.35 mm and 2000 Hz. The results are shown in Fig. 12. The overall heat transfer for the fin channel was calculated in an area-weighted sense:

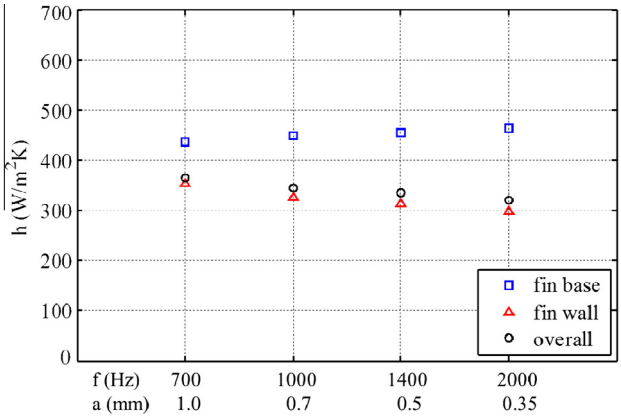

Fig. 12. Heat transfer coefficients with a constant amplitude–frequency product.

$$h = \frac{(hs)_{leftwall} + (hs)_{base} + (hs)_{rightwall}}{s_{leftwall} + s_{base} + s_{rightwall}} \tag{6}$$

where *s* is heat transfer area of each surface. Heat transfer coefficients on the base surface show slightly larger sensitivity to frequency, but heat transfer coefficients on the side walls show larger sensitivity to amplitude. Overall heat transfer coefficients are slightly more sensitive to the amplitude.

The opposite trends of heat transfer coefficients for the base surface vs. the side walls may be understood via Fig. 13 in which contours of TKE on the same *XY* and *YZ* planes are plotted for two of the four cases. At the instant shown, the plate is at its neutral position and is about to move toward the right. The contours indicate that at low frequency and large amplitude (Fig. 13(a)), the turbulence is not so strong but is transported over a larger region, while at high frequency and small amplitude (Fig. 13(b)), the turbulence is stronger but is limited to a region more local to the top edge of the agitator plate. Similar features are observed at different times within an operational cycle. Consequently, the more diffuse turbulence increases the heat transfer coefficients on the side walls as the amplitude increases, whereas the localized strong turbulence increases heat transfer coefficients on the base wall as frequency increases. Since the fin side walls account for the dominant portion of the total heat transfer surface area of the channel, the overall heat transfer increases as the amplitude increases.

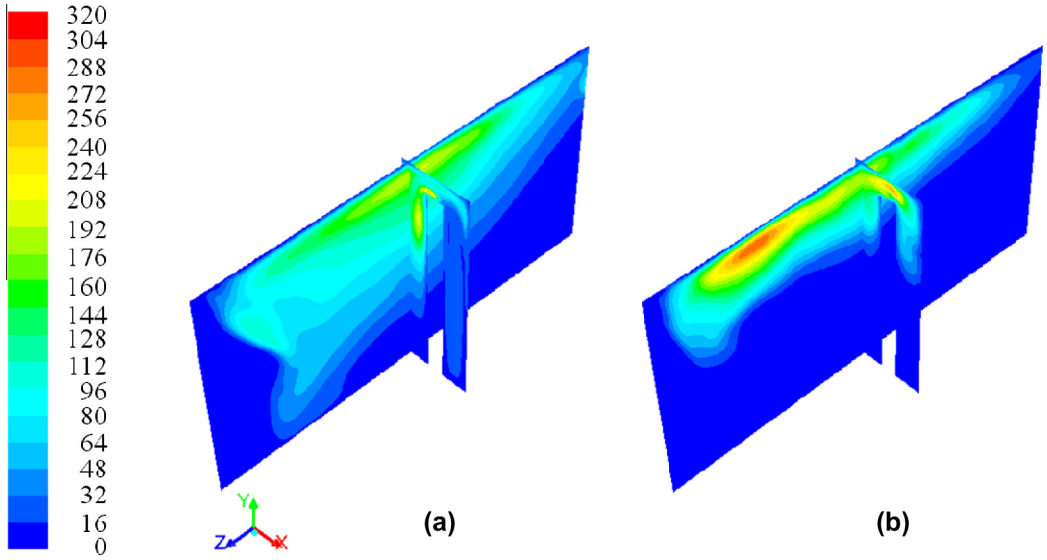

Fig. 13. Contours of TKE [m^2/s^2] on the same *XY* and *YZ* planes at the beginning of a cycle; (a) 1.0 mm and 700 Hz, (b) 0.35 mm and 2000 Hz.

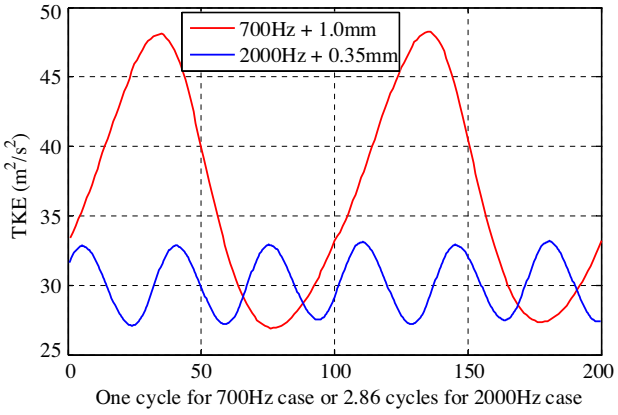

Fig. 14. Variation of volumetric-averaged TKE over an equal time interval for the 1.00 mm and 700 Hz case and the 0.35 mm and 2000 Hz case.

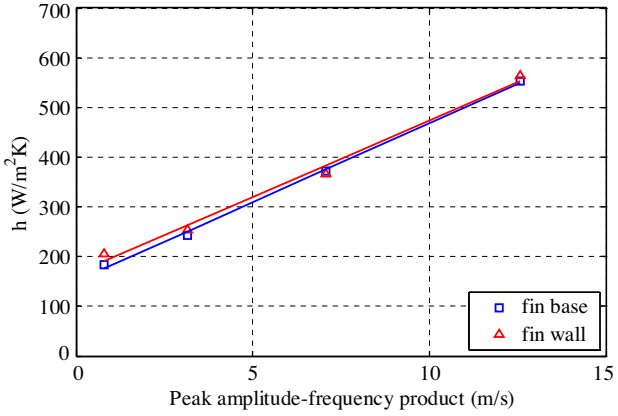

Fig. 15. Heat transfer coefficients with different amplitude–frequency products; solid lines are linear fits to data.

Fig. 14 shows volumetric-averaged TKE over an equal time interval for the two cases presented in Fig. 13. The TKE variation is slow, but large, for the low-frequency, large-amplitude case and is fast, but small, for the high-frequency, small-amplitude case. The average TKE over the time interval is 36.6 m^2/s^2 for the former case and 30.2 m^2/s^2 for the latter case, which confirms that heat transfer with large amplitude and low frequency is slightly higher than with small amplitude and high frequency.

Effects of increasing amplitude-frequency product on heat transfer enhancement were investigated in the translational mode with 2.5 mm tip gap size. The amplitude and frequency were varied as 0.25 mm and 500 Hz, 0.50 mm and 1000 Hz, 0.75 mm and 1500 Hz, and 1.00 mm and 2000 Hz. The corresponding peak agitation velocities, $2\pi Af$, are 0.79, 3.14, 7.07, and 12.57 m/s, respectively. Fig. 15 shows heat transfer coefficients vs. peak agitation velocity. Heat transfer coefficients on both the base and side walls linearly increase as the amplitude–frequency product increases. This is because the tip gap size is 2.5 mm, close to the 2.6 mm total plate-to-side-wall spacing. As discussed in the section regarding the tip gap size effects, heat transfer on the base and side walls are the same when the tip gap size is equal to the total plate-to-side-wall spacing (Fig. 8).

Heat transfer enhancement on the base and side walls are directly related to the changes in amplitude–frequency product (the peak agitation velocity). To enhance heat transfer on the channel surfaces, the foremost effort with an agitator plate is to raise the peak agitation velocity. This is limited by the power available for agitation. Amplitude is shown to be slightly more influential than frequency for a fixed amplitude–frequency product, but this effect is secondary.

5. Conclusions

Integration of agitator plates with air-cooled heat sinks to enhance heat transfer has been computationally investigated. This was conducted by using a single channel constructed by two sidewalls and one base wall with a single agitator plate within the channel. Air flows through the channel while the plate vibrates in the transverse direction to agitate the flow. Operational parameters, such as the operational mode, the tip gap size between the plate and the base wall, and the operational amplitude and frequency of the agitator plate all significantly change the air flow inside the channel and, accordingly, augment heat transfer.

Periodic transverse motion of the agitator plate generates turbulence mainly over its moving edge. Turbulence generated is carried to the base and side walls, resulting in substantial heat transfer enhancement over the heat transfer surfaces, up to 139%

on the base wall and 61% on the side walls, compared with un-agitated channel flow.

Turbulence generated by a flapping agitator plate is weaker and affects a smaller portion of the flow field than that generated by a translational agitator plate. The resultant heat transfer enhancement by the flapper is consequently lower than that by the translator, by 23% on the fin base and 33% on the side walls.

Heat transfer on the fin base is sensitive to tip gap size, decreasing sharply with increasing tip gap sizes. Heat transfer on the side walls is essentially insensitive to the tip gap size.

Heat transfer on the fin base and side walls increases linearly as operational amplitude or frequency increases. Given a constant amplitude–frequency product, the amplitude is slightly more significant than is the frequency. An increasing amplitude–frequency product is the primary operational parameter for heat transfer enhancement.

Acknowledgments

This work was supported in part by the Defense Advanced Research Projects Agency (DARPA) Microtechnologies for Air-Cooled Exchangers (MACE) Program. The views expressed are those of the authors and do not reflect the official policy or position of the Department of Defense or the U.S. Government. This work is approved for public release and unlimited distribution. The authors also acknowledge computational resources and technical consultation from the Minnesota Supercomputing Institute at the University of Minnesota.

References

[1] P. Teertstra, M.M. Yovanovich, J.R. Culham, Analytical forced convection modeling of plate fin heat sinks, J. Electron. Manuf. 10 (4) (2000) 253–261.
[2] Z. Duan, Y.S. Muzychka, Experimental investigation of heat transfer in impingement air cooled plate fin heat sinks, ASME J. Electron. Packag. 128 (4) (2006) 412–418.
[3] E.M. Sparrow, D.S. Kadle, Effect of tip-to-shroud clearance on turbulent heat transfer from a shrouded, longitudinal fin array, ASME J. Heat Transfer 108 (3) (1986) 519–524.
[4] S.A. El-Sayed, S.M. Mohamed, A.M. Abdel-latif, A.E. Abouda, Investigation of turbulent heat transfer and fluid flow in longitudinal rectangular-fin arrays of different geometries and shrouded fin array, Exp. Therm. Fluid Sci. 26 (8) (2002) 879–900.
[5] M. Saini, R.L. Webb, Heat rejection limits of air cooled plane fin heat sinks for computer cooling, IEEE Trans. Compon. Packag. Technol. 26 (1) (2003) 71–79.
[6] R.J. Moffat, Modeling air-cooled heat sinks as heat exchangers, in: Proceedings of IEEE 23rd Semiconductor Thermal Measurement and Management Symposium, San Jose, California, USA, 2007, pp. 200–207.
[7] A. Ortega, P. Skandakumaran, B. Hassell, A modified effectiveness-ntu approach for analysis of low-aspect ratio mini-channel heat sinks using novel shape factor formulations, in: Proceedings of IEEE Intersociety Conference on Thermal and Thermomechanical Phenomena in Electronic Systems, Orlando, Florida, 2008, pp. 167–173.
[8] A. Bar-Cohen, I. Madhusudan, Design and optimization of air-cooled heat sinks for sustainable development, IEEE Trans. Compon. Packag. Technol. 25 (4) (2002) 584–591.
[9] P. Rodgers, V. Eveloy, M.G. Pecht, Limits of air-cooling: status and challenges, in: Proceedings of IEEE 21st Semiconductor Thermal Measurement and Management Symposium, San Jose, California, USA, 2005, pp. 116–124.
[10] M. Toda, Theory of air flow generation by a resonant type PVF_2 bimorph cantilever vibrator, Ferroelectrics 22 (1979) 911–918.
[11] M. Joshi, S. Priva, Piezo-bow-high displacement and high blocking force actuator, Integr. Ferroelectr. 82 (1) (2006) 25–43.
[12] Y.-H. Kim, S.T. Wereley, C.-H. Chun, Phase-resolved flow field produced by a vibrating cantilever plate between two endplates, Phys. Fluids 16 (1) (2004) 145–162.
[13] A. Eastman, M. Kimber, Flow filed analysis of a single piezoelectric fan, in: Proceedings of ASME 2009 International Mechanical Engineering Congress and Exposition, vol. 9, issue part B, Lake Buena Vista, Florida, USA, 2009, pp. 1429–1436.
[14] R.R. Schmidt, Local and average transfer coefficients on a vertical surface due to convection from a piezoelectric fan, in: Proceedings of IEEE Intersociety Conference on Thermal Phenomena in Electronic Systems, Washington, DC, USA, 1994, pp. 41–49.
[15] M. Kimber, S.V. Garimella, A. Raman, Local heat transfer coefficients induced by piezoelectrically actuated vibrating cantilevers, ASME J. Heat Transfer 129 (9) (2007) 1168–1176.
[16] M. Kimber, S.V. Garimella, Measurement and prediction of the cooling characteristics of a generalized vibrating piezoelectric fan, Int. J. Heat Mass Transfer 52 (19–20) (2009) 4470–4478.
[17] M. Kimber, S.V. Garimella, Cooling performance of arrays of vibrating cantilevers, ASME J. Heat Transfer 131 (11) (2009) 1401–1408.
[18] S.-F. Liu, R.-T. Huang, W.-J. Sheu, C.-C. Wang, Heat transfer by a piezoelectric fan on a flat surface subject to the influence of horizontal/vertical arrangement, Int. J. Heat Mass Transfer 52 (11–12) (2009) 2565–2570.
[19] T. Açıkalın, S.V. Garimella, A. Raman, J. Petroski, Characterization and optimization of the thermal performance of miniature piezoelectric fans, Int. J. Heat Fluid Flow 28 (4) (2007) 806–820.
[20] M.K. Abdullah, M.Z. Abdullah, M.V. Ramana, C.Y. Khor, K.A. Ahmad, M.A. Mujeebu, Y. Ooi, Z. Mohd Ripin, Numerical and experimental investigations on effect of fan height on the performance of piezoelectric fan in microelectronic cooling, Int. Commun. Heat Mass Transfer 36 (1) (2009) 51–58.
[21] C.-N. Lin, Analysis of three-dimensional heat and fluid flow induced by piezoelectric fan, Int. J. Heat Mass Transfer 55 (11–12) (2012) 3043–3053.
[22] J. Petroski, M. Arik, M. Gursoy, Optimization of piezoelectric oscillating fan-cooled heat sinks for electronics cooling, IEEE Trans. Compon. Packag. Technol. 33 (1) (2010) 25–31.
[23] H.K. Ma, H.C. Su, C.L. Liu, W.H. Ho, Investigation of a piezoelectric fan embedded in a heat sink, Int. Commun. Heat Mass Transfer 39 (5) (2012) 603–609.
[24] M.K. Abdullah, N.C. Ismail, M.Z. Abdullah, M. Abdul Mujeebu, K.A. Ahmad, Z. Mohd Ripin, Effects of tip gap and amplitude of piezoelectric fans on the performance of heat sinks in microelectronic cooling, Heat Mass Transfer 48 (6) (2012) 893–901.
[25] M.K. Abdullah, N.C. Ismail, M. Abdul Mujeebu, M.Z. Abdullah, K.A. Ahmad, Muhamad Husaini, M.N.A. Hamid, Optimum tip gap and orientation of multi-piezofan for heat transfer enhancement of finned heat sink in microelectronic cooling, Int. J. Heat Mass Transfer 55 (21–22) (2012) 5514–5525.
[26] H.K. Ma, H.C. Su, W.F. Luo, Investigation of a piezoelectric fan cooling system with multiple magnetic fans, Sens. Actuators A 189 (1) (2013) 356–363.
[27] T. Yeom, T. Simon, Y. Yu, M. North, T. Cui, Convective heat transfer enhancement on a channel wall with a high frequency, oscillating agitator, in: Proceedings of ASME 2011 International Mechanical Engineering Congress and Exposition, Denver, Colorado, USA, 2011.
[28] Y. Yu, T. Simon, M. Zhang, T. Yeom, M. North, T. Cui, Enhancing heat transfer of air-cooled heat sinks using piezoelectrically-driven agitators and synthetic jets, in: Proceedings of ASME 2011 International Mechanical Engineering Congress and Exposition, Denver, Colorado, USA, 2011.
[29] T. Yeom, T.W. Simon, M. Zhang, M.T. North, T. Cui, High frequency, large displacement, and low power consumption piezoelectric translational actuator based on an oval loop shell, Sens. Actuators A 176 (4) (2012) 99–109.
[30] T. Yeom, T.W. Simon, L. Huang, M.T. North, T. Cui, Piezoelectric translational agitation for enhancing forced-convection channel-flow heat transfer, Int. J. Heat Mass Transfer 55 (25–26) (2012) 7398–7409.
[31] ANSYS FLUENT 13.0, Ansys, Inc., Canonsburg, Pennsylvania, USA.
[32] Y. Yu, T. Simon, M. North, T. Cui, Comparison of heat transfer enhancement by actuated plates in heat-sink channels, in: Proceedings of ASME 2012 Summer Heat Transfer Conference, Puerto Rico, USA, 2012.